ChemComm

COMMUNICATION

View Article Online
View Journal | View Issue

Cite this: *Chem. Commun.*, 2015, **51**, 13515

Received 12th May 2015,
Accepted 16th July 2015

DOI: 10.1039/c5cc03917g

www.rsc.org/chemcomm

(3*E*,8*E*)-3,8-Bis(2-oxoindolin-3-ylidene)naphtho-[1,2-*b*:5,6-*b*′]difuran-2,7(3*H*,8*H*)-dione (INDF) based polymers for organic thin-film transistors with highly balanced ambipolar charge transport characteristics†

Yunfeng Deng, Bin Sun, Yinghui He, Jesse Quinn, Chang Guo and Yuning Li*

Two donor–acceptor (D–A) conjugated polymers, PINDFTT and PINDFBT, based on a novel electron acceptor, (3*E*,8*E*)-3,8-bis(2-oxoindolin-3-ylidene)naphtho-[1,2-*b*:5,6-*b*′]difuran-2,7(3*H*,8*H*)-dione (INDF), are synthesized for solution processed organic thin-film transistors. Both polymers exhibited highly balanced ambipolar characteristics with hole and electron mobilities up to 0.51 cm^2 V^{-1} s^{-1} and 0.50 cm^2 V^{-1} s^{-1}, respectively.

Organic thin-film transistors (OTFTs) have received tremendous attention from academia and industries due to their competitive advantages such as low-cost, light-weight, and flexibility over silicon-based transistors.[1–3] Recently, significant progress has been made in the development of high-performance unipolar polymer semiconductors, exhibiting p-channel or n-channel mobilities exceeding commercially viable values.[4–17] Ambipolar polymer semiconductors, which uniquely show both p-type and n-type channel performances in one device depending on the applied voltages, are potentially useful as single-component semiconductors to simplify the fabrication process for complementary metal oxide semiconductor (CMOS)-like circuits.[18,19] To be qualified for the CMOS-like logic circuits, a critical requirement is that the ambipolar polymer should have well-balanced p- and n-channel operation characteristics.

It is believed that one key factor for achieving balanced ambipolar charge transport performance of a polymer semiconductor is to obtain suitable energy levels of the highest occupied molecular orbitals (HOMOs) and the lowest unoccupied molecular orbitals (LUMOs) that have small and balanced energy barriers with respect to the Fermi energy of the source contact conductor.[19] Another critical requirement is that the LUMO and HOMO energy levels of the polymer should be below *ca.* −3.7 to −4.0 eV[20–23] and −5.0 eV[20,21] to realize stable n-channel and p-channel operations, respectively. In recent years, the combination of electron donating (D) and electron accepting (A) building blocks into the polymer main chain has proven to be one of the most effective strategies to construct ambipolar polymer semiconductors because the energy levels of D–A copolymers can be fine-tuned by choosing different D and A units.[17,24–28]

Recently, our group reported a new strong electron accepting building block, (3*E*,7*E*)-3,7-bis(2-oxoindolin-3-ylidene)benzo-[1,2-*b*:4,5-*b*′]difuran-2,6(3*H*,7*H*)-dione (IBDF).[29] This acceptor unit has a large symmetric and planar fused ring structure, which would increase the π–π overlap and intermolecular interaction. Due to the strong electron-accepting ability of the IDBF unit, IBDF-based polymers exhibited unipolar n-type characteristics with high electron mobilities exceeding 1 cm^2 V^{-1} s^{-1}.[12] In some cases, when a strong donor unit is used, ambipolar charge performance could be obtained, but the electron transport is dominant over the hole transport.[20,30,31] In this work, we synthesized a new acceptor unit, namely, (3*E*,8*E*)-3,8-bis(2-oxoindolin-3-ylidene)naphtho-[1,2-*b*:5,6-*b*′]difuran 2,7(3*H*,8*H*)-dione (INDF), by replacing the benzene ring in IBDF with the naphthalene ring. Compared with benzene, naphthalene is larger in size with a more extended π-system, which would further facilitate the π–π overlap and intermolecular interaction. More important is that the large central naphthalene moiety would result in a weaker electron-accepting ability in INDF compared with IBDF, which may help to realize balanced electron and hole mobilities. Our predicted computer simulation results showed that the INDF monomer and dimer indeed possess higher LUMO and HOMO energy levels compared with the corresponding IBDF monomer and dimer, respectively. Two new polymers based on this new acceptor, **PINDFTT** and **PINDFBT**, were synthesized and used as semiconductors for OTFTs. As we expected, both polymers showed highly balanced ambipolar transport characteristics (the ratio of hole and electron mobilities, $\mu_h/\mu_e \approx 1$). The highest hole and electron mobilities of 0.51 cm^2 V^{-1} s^{-1} and 0.50 cm^2 V^{-1} s^{-1}, respectively, were achieved.

Scheme 1 illustrates the synthetic route to an INDF-based monomer and its polymers. The reaction of the sodium salt of **1**

Department of Chemical Engineering and Waterloo Institute for Nanotechnology (WIN), 200 University Ave W, Waterloo, Ontario, N2L3G1, Canada.
E-mail: yuning.li@uwaterloo.ca; Fax: +1 519-888-4347;
Tel: +1 519-888-4567 ext. 31105

† Electronic supplementary information (ESI) available: Synthetic procedures, device fabrication, and additional data. See DOI: 10.1039/c5cc03917g

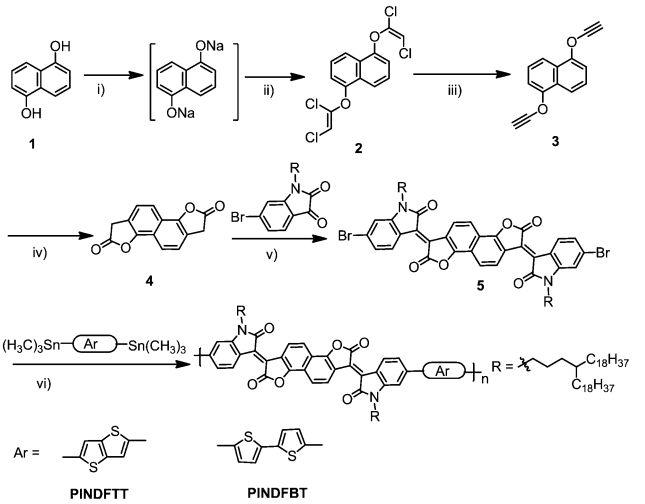

Scheme 1 Synthesis route to the INDF monomer and polymers: (i) NaOH, DMSO, r.t.; (ii) 1,1,2-trichloroethylene, r.t.; (iii) *n*-BuLi, Et_2O, −78 °C to −40 °C; (iv) 2,6-dimethylpyridine *N*-oxide, $HBF_4{\cdot}Et_2O$, 1,4-dioxane, 80 °C; (v) *p*-TsOH, AcOH, 115 °C; (vi) $Pd_2(dba)_3$/P(*o*-tolyl)$_3$, chlorobenzene, 130 °C.

with 1,1,2-trichloroethylene proceeded to give **2**, which was treated with *n*-butyl lithium at −40 °C to form **3**. Crude **3** was subjected to an oxidative cyclization reaction using HBF_4 diethyl etherate as a catalyst and 2,6-dimethylpyridine *N*-oxide as an oxidant to provide **4**. Direct condensation of **4** and two equivalents of 6-bromo-1-(4-octadecyldocosan)indoline-2,3-dione in acetic acid with a catalytic amount of *p*-toluenesulfonic acid afforded monomer **5**. Previously we found that a branched side chain, 2-decyltetradecyl, is inadequate for solubilizing the IBDF–BT copolymer.[29] Because the solubility of INDF polymers was expected to be poorer than that of the IBDF polymers, we used the very large 4-octadecyldocosan side chain[12,13,30,31] to render the INDF polymers soluble. **PINDFTT** and **PINDFBT** with thieno[3,2-*b*]thiopehne (TT) and bithiophene (BT) as donor units, respectively, were prepared through the Stille-coupling polymerization using the $Pd_2(dba)_3$/P(*o*-tolyl)$_3$ catalyst system. **PINDFTT** is soluble in common chlorinated solvents such as chloroform, 1,1,2,2-tetrachloroethane, chlorobenzene and 1,2-dichlorobenzene. However, **PINDFBT** can only be dissolved in hot 1,2-dichlorobenzene. The molecular weights of the polymers were characterized by high temperature gel permeation chromatography (HT-GPC) at 140 °C using 1,2,4-tricholorobenzene as the eluent and polystyrene as standard. The number average molecular weight (M_n) and polydispersity index (PDI) are 27.6 kDa and 4.9 for **PINDFTT**, and 43.1 kDa and 4.8 for **PINDFBT**. Both polymers showed excellent thermal stability with the 5% weight loss at a temperature of ~380 °C, as revealed by thermal gravimetric analysis (TGA, Fig. S10, ESI†).

Fig. 1 shows the UV-vis-NIR absorption spectra of polymers in *o*-dichlorobenzene (*o*-DCB) solutions and solid thin films. Both polymers exhibited dual band absorption, which is typical for the D–A conjugated systems. In dilute solutions, the maximum absorption wavelengths (λ_{max}) for **PINDFTT** and **PINDFBT** are 787 nm and 816 nm, respectively. Going from solution to the solid state, the λ_{max} of both polymers blueshifted (≈10 nm), which might be induced by the H-aggregation-type inter-chain

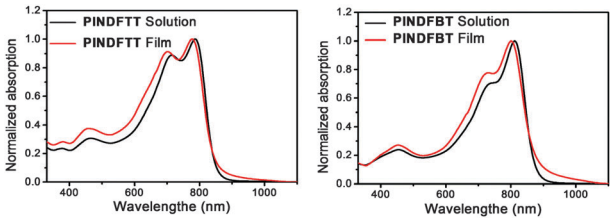

Fig. 1 The UV-vis-IR absorption spectra of **PINDFTT** (left) and **PINDFBT** (right) in *o*-DCB solution and film.

packing in the solid state.[32,33] The same phenomenon was also observed in some other D–A polymers.[23,34] The optical band-gaps (E_g^{opt}) deduced from the absorption edges of the film spectra are 1.45 eV and 1.41 eV for **PINDFTT** and **PINDFBT**, respectively. In comparison with the IBDF polymers, the INDF polymer showed blue-shifted λ_{max}, which might be due to the less electron-accepting capability of the INDF building block (see discussions below), resulting in weaker intra- and inter-molecular D–A interactions.

Cyclic voltammetry (CV) measurements were performed on polymer films to estimate the energy levels of the polymers (ESI,† Fig. S13). By using the oxidative onset potentials, the HOMO energy levels were calculated to be −5.76 eV and −5.65 eV for **PINDFTT** and **PINDFBT**, respectively. The LUMO energy levels were calculated from the reduction onset potentials to be −3.79 eV and −3.84 eV for **PINDFTT** and **PINDFBT**, respectively. The band gaps calculated from the CV results are 1.97 eV for **PINDFTT** and 1.81 eV for **PINDFBT**, which are much larger than their optical band gaps. These discrepancies are due to the large exciton binding energy frequently observed for polymer semiconductors.[23,35,36] Compared with the reported IBDF-based polymers with the same donor units, namely, **PIBDFTT** and **PIBDFBT** (see their structures and energy levels in Fig. S14, ESI†),[30,31] the HOMO and LUMO energy levels of **PINDFTT** and **PINDFBT** have been raised, which would be beneficial for more balanced hole and electron injection when gold contacts are used. According to the above results, the INDF polymers have shown larger band-gaps, higher HOMO and LUMO energy levels compared to the IBDF polymers, indicating that the INDF unit has a weaker electron-withdrawing ability relative to the IBDF moiety.

To gain insight into the geometry and electronic distribution of these INDF polymers, computer simulations were performed on the INDF unit and the dimer units ((INDF-TT)$_2$ and (INDF-BT)$_2$) of these polymers, where a short alkyl, methyl, was used to reduce the computational time (Fig. S15–S17, ESI†). The corresponding structures based on IBDF were also analysed for comparison. The results showed that the dihedral angle between an indolin-2-one unit and the naphtho-[1,2-*b*:5,6-*b*′]difuran-2,7(3*H*,8*H*)-dione core in INDF for the INDF compounds is ~11–13°, which is slightly larger than the dihedral angle between the indolin-2-one and the benzo[1,2-*b*:4,5-*b*′]difuran-2,6(3*H*,7*H*)-dione core in the IBDF compounds (~8°). This may be another reason causing the blue-shifted optical absorption of the INDF-based polymers compared to the IBDF polymers. The HOMO and LUMO energy levels of these small molecule INDF compounds are higher than those

of the corresponding IBDF compounds, which is consistent with our electrochemical results for the polymers.

Bottom-gate, bottom-contact (BGBC) OTFT devices on an n^{++}-doped silicon wafer with a 300 nm thermally grown SiO_2 layer were used to evaluate the performance of **PINDFTT** and **PINDFBT**. The substrate was pre-patterned with gold source and drain pairs and the SiO_2 surface was modified with dodecyltrichlorosilane (DDTS) to minimize the surface charge trapping. The semiconducting layer was deposited by spin-coating a polymer solution onto the substrate. Both polymers showed ambipolar charge transport characteristics (Table S1, ESI†). For devices based on **PINDFTT**, the best performance with a hole mobility of 0.10 $cm^2\ V^{-1}\ s^{-1}$ and an electron mobility of 0.11 $cm^2\ V^{-1}\ s^{-1}$ was achieved for the 150 °C-annealed film (ESI†). After annealing at a higher temperature of 200 °C, the hole and electron mobilities increased slightly up to 0.12 $cm^2\ V^{-1}\ s^{-1}$ and 0.14 $cm^2\ V^{-1}\ s^{-1}$, respectively (Fig. S18, ESI†). The devices based on **PINDFBT** showed much better performance with the average hole and electron mobilities of 0.38 $cm^2\ V^{-1}\ s^{-1}$ and 0.34 $cm^2\ V^{-1}\ s^{-1}$ for the 150 °C-annealed film. The best performing device showed hole and electron mobilities of 0.51 $cm^2\ V^{-1}\ s^{-1}$ and 0.50 $cm^2\ V^{-1}\ s^{-1}$, respectively, for a 150 °C-annealed film (Fig. 2). Annealing at temperatures higher than 200 °C did not improve device performances. It should be emphasized that both polymers exhibited highly balanced hole and electron transport characteristics with the μ_h/μ_e ratio close to 1. The favourably positioned HOMO and LUMO levels of these polymers with respect to the Fermi level of gold (~−4.5 to −5.1 eV)[37,38] would have created similar hole and electron injection barriers, which might account for their highly balanced hole and electron transport performance. We noticed that **PINDFTT** showed lower charge transport performance than **PINDFBT**. This discrepancy might be caused by their different energy levels. Compared to **PINDFBT**, **PINDFTT** has a lower HOMO energy level and higher LUMO energy level, creating higher injection barriers for both hole and electron.

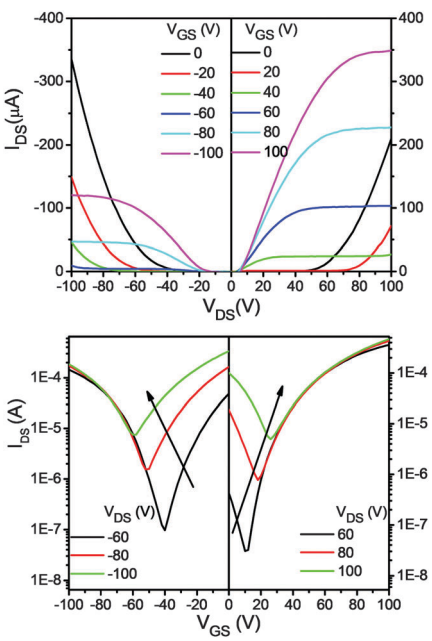

Fig. 2 Output (top) and transfer (bottom) curves of an OTFT device based on a thin film of **PINDFBT** annealed at 150 °C.

The thin film crystallinity of the two polymers was investigated using X-ray diffraction (XRD). As shown in Fig. S19 (ESI†), thin films of both polymers spin-coated on modified SiO_2/Si substrates clearly showed a primary peak (100) at 2θ = 3.1°, which corresponds to a *d*-spacing of 2.84 nm. It is noted that there is no reflection peak around ~20–25° that represents the typical π–π stacking distance. This indicated that the polymer backbones adopted an edge-on orientation motif respective to the substrates, which is beneficial for charge transportation in OTFT devices.[2,39] After annealing at 150 °C, the intensity of the primary peak for both polymers became stronger, but the improvement in crystallinity for **PINDFBT** is more evident. A small peak at 2θ = 6.3° is also observed for both polymers, which is assigned to the secondary reflection peak (200). When the annealing temperature was further increased to 200 °C, the intensity of the primary peak for **PINDFTT** was further enhanced and the secondary peak became more pronounced. On the other hand, the 200 °C-annealed **PINDFBT** film showed insignificant changes in the diffraction intensity, suggesting that high crystallinity was already achieved for this polymer at an annealing temperature of 150 °C. The dependence of crystallinity on the annealing temperature is in good agreement with the OTFT results. The AFM height images of the films are shown in Fig. S20 and S21 (ESI†). All of the **PINDFTT** films are quite smooth with a root-mean-square roughness (R_q) of ~1.7 nm. The surface morphology was not significantly influenced by thermal annealing. The morphology and roughness of the **PINDFBT** films remained similar when the annealing temperature was increased from 100 °C (R_q = 1.2 nm) to 150 °C (R_q = 1.4 nm). However, the 200 °C-annealed film showed large fibre-like bundles and became rougher (R_q = 3.4 nm).

In summary, we reported a novel electron-accepting building block, INDF, and two INDF-based D–A conjugated polymers, **PINDFTT** and **PINDFBT**. Compared to the IBDF-based polymers, the INDF-based polymers exhibited larger band-gaps, higher HOMO and LUMO energy levels due to the weaker electron-accepting property of INDF relative to that of IBDF. The INDF-polymers exhibited highly balanced ambipolar characteristics with the highest hole and electron mobilities of 0.51 $cm^2\ V^{-1}\ s^{-1}$ and 0.50 $cm^2\ V^{-1}\ s^{-1}$, respectively. Our preliminary results demonstrated that INDF is a very promising electron acceptor building block for polymer semiconductors for ambipolar OTFTs and other printed electronics.

The authors thank the Natural Sciences and Engineering Research Council (NSERC) of Canada for the financial support (Discovery Grants #402566-2011) of this work.

Notes and references

1 C. Wang, H. Dong, W. Hu, Y. Liu and D. Zhu, *Chem. Rev.*, 2012, **112**, 2208–2267.
2 Y. Li, P. Sonar, L. Murphy and W. Hong, *Energy Environ. Sci.*, 2013, **6**, 1684–1710.
3 J. Mei and Z. Bao, *Chem. Mater.*, 2014, **26**, 604–615.
4 H. N. Tsao, D. M. Cho, I. Park, M. R. Hansen, A. Mavrinskiy, D. Y. Yoon, R. Graf, W. Pisula, H. W. Spiess and K. Müllen, *J. Am. Chem. Soc.*, 2011, **133**, 2605–2612.

5 J. Mei, D. H. Kim, A. L. Ayzner, M. F. Toney and Z. Bao, *J. Am. Chem. Soc.*, 2011, **133**, 20130–20133.
6 J. Li, Y. Zhao, H. S. Tan, Y. Guo, C.-A. Di, G. Yu, Y. Liu, M. Lin, S. H. Lim, Y. Zhou, H. Su and B. S. Ong, *Sci. Rep.*, 2012, **2**, 754.
7 I. Kang, H.-J. Yun, D. S. Chung, S.-K. Kwon and Y.-H. Kim, *J. Am. Chem. Soc.*, 2013, **135**, 14896–14899.
8 T. Lei, J.-H. Dou and J. Pei, *Adv. Mater.*, 2012, **24**, 6457–6461.
9 Y. Li, P. Sonar, S. P. Singh, M. S. Soh, M. van Meurs and J. Tan, *J. Am. Chem. Soc.*, 2011, **133**, 2198–2204.
10 T. Lei, J.-H. Dou, Z.-J. Ma, C.-H. Yao, C.-J. Liu, J.-Y. Wang and J. Pei, *J. Am. Chem. Soc.*, 2012, **134**, 20025–20028.
11 B. Sun, W. Hong, H. Aziz, N. M. Abukhdeir and Y. Li, *J. Mater. Chem. C*, 2013, **1**, 4423–4426.
12 T. Lei, J.-H. Dou, X.-Y. Cao, J.-Y. Wang and J. Pei, *J. Am. Chem. Soc.*, 2013, **135**, 12168–12171.
13 T. Lei, X. Xia, J.-Y. Wang, C.-J. Liu and J. Pei, *J. Am. Chem. Soc.*, 2014, **136**, 2135–2141.
14 B. Sun, W. Hong, Z. Yan, H. Aziz and Y. Li, *Adv. Mater.*, 2014, **26**, 2636–2642.
15 Y. Deng, Y. Chen, X. Zhang, H. Tian, C. Bao, D. Yan, Y. Geng and F. Wang, *Macromolecules*, 2012, **45**, 8621–8627.
16 G. Kim, S.-J. Kang, G. K. Dutta, Y.-K. Han, T. J. Shin, Y.-Y. Noh and C. Yang, *J. Am. Chem. Soc.*, 2014, **136**, 9477–9483.
17 J. Lee, A. R. Han, H. Yu, T. J. Shin, C. Yang and J. H. Oh, *J. Am. Chem. Soc.*, 2013, **135**, 9540–9547.
18 H. Chen, Y. Guo, Z. Mao, G. Yu, J. Huang, Y. Zhao and Y. Liu, *Chem. Mater.*, 2013, **25**, 3589–3596.
19 S. Z. Bisri, C. Piliego, J. Gao and M. A. Loi, *Adv. Mater.*, 2014, **26**, 1176–1199.
20 G. Zhang, P. Li, L. Tang, J. Ma, X. Wang, H. Lu, B. Kang, K. Cho and L. Qiu, *Chem. Commun.*, 2014, **50**, 3180–3183.
21 J. Zaumseil and H. Sirringhaus, *Chem. Rev.*, 2007, **107**, 1296–1323.
22 L. Wang, X. Zhang, H. Tian, Y. Lu, Y. Geng and F. Wang, *Chem. Commun.*, 2013, **49**, 11272–11274.
23 Y. He, C. Guo, B. Sun, J. Quinn and Y. Li, *Chem. Commun.*, 2015, **51**, 8093–8096.
24 K.-J. Baeg, M. Caironi and Y.-Y. Noh, *Adv. Mater.*, 2013, **25**, 4210–4244.
25 P. Sonar, S. P. Singh, Y. Li, M. S. Soh and A. Dodabalapur, *Adv. Mater.*, 2010, **22**, 5409–5413.
26 J. D. Yuen, J. Fan, J. Seifter, B. Lim, R. Hufschmid, A. J. Heeger and F. Wudl, *J. Am. Chem. Soc.*, 2011, **133**, 20799–20807.
27 W. Hong, B. Sun, H. Aziz, W.-T. Park, Y.-Y. Noh and Y. Li, *Chem. Commun.*, 2012, **48**, 8413–8415.
28 B. Sun, W. Hong, H. Aziz and Y. Li, *Polym. Chem.*, 2015, **6**, 938–945.
29 Z. Yan, B. Sun and Y. Li, *Chem. Commun.*, 2013, **49**, 3790–3792.
30 T. Lei, J.-H. Dou, X.-Y. Cao, J.-Y. Wang and J. Pei, *Adv. Mater.*, 2013, **25**, 6589–6593.
31 X. Zhou, N. Ai, Z.-H. Guo, F.-D. Zhuang, Y.-S. Jiang, J.-Y. Wang and J. Pei, *Chem. Mater.*, 2015, **27**, 1815–1820.
32 X. Zhang, J. P. Johnson, J. W. Kampf and A. J. Matzger, *Chem. Mater.*, 2006, **18**, 3470–3476.
33 H. Hwang, D. Khim, J.-M. Yun, E. Jung, S.-Y. Jang, Y. H. Jang, Y.-Y. Noh and D.-Y. Kim, *Adv. Funct. Mater.*, 2015, **25**, 1146–1156.
34 J. Shin, H. A. Um, D. H. Lee, T. W. Lee, M. J. Cho and D. H. Choi, *Polym. Chem.*, 2013, **4**, 5688–5695.
35 Y. Zhu, R. D. Champion and S. A. Jenekhe, *Macromolecules*, 2006, **39**, 8712–8719.
36 Y. Deng, Y. Chen, J. Liu, L. Liu, H. Tian, Z. Xie, Y. Geng and F. Wang, *ACS Appl. Mater. Interfaces*, 2013, **5**, 5741–5747.
37 S. Braun, W. R. Salaneck and M. Fahlman, *Adv. Mater.*, 2009, **21**, 1450–1472.
38 A. Wan, J. Hwang, F. Amy and A. Kahn, *Org. Electron.*, 2005, **6**, 47–54.
39 H. Sirringhaus, P. J. Brown, R. H. Friend, M. M. Nielsen, K. Bechgaard, B. M. W. Langeveld-Voss, A. J. H. Spiering, R. A. J. Janssen, E. W. Meijer, P. Herwig and D. M. de Leeuw, *Nature*, 1999, **401**, 685–688.

